Available online at www.sciencedirect.com
ScienceDirect
Catalysis Today 120 (2007) 420–425
CATALYSIS TODAY
www.elsevier.com/locate/cattod

The adsorption properties of surface modified activated carbon fibers for hydrogen storages

Young Seak Lee [a,*], Young Ho Kim [a], Ji Sook Hong [b], Jeong Kwon Suh [b], Gyou Jin Cho [c]

[a] *Department of Fine Chemical Engineering & Chemistry, BK21-E²M, Chungnam National University, Daejeon 305-764, Republic of Korea*
[b] *Korea Research Institute of Chemical Technology, Daejeon 305-600, Republic of Korea*
[c] *Department Chemical Engineering, Sunchon National University, Chonnam 540-742, Republic of Korea*

Available online 13 November 2006

Abstract

In this study, activated carbon fibers (ACFs) with high surface area and pore volume have been modified by Ni doping and fluorination. The surface modified ACFs were characterized by BET surface area, SEM/EDS, XRD, and Raman spectroscopy. The changes in pore structure and surface properties of these modified ACFs were correlated with hydrogen storage capabilities. After fluorination treatment, although the micropore volume of ACF was decreased, amounts of hydrogen storage were found to increase. Additionally, micropore volume on ACFs was found to be unchanged with Ni doping, hydrogen storage capacities were considerably increased due to the effect of catalytic activation of nickel. Though fluorination of ACFs increases hydrogen affinity, the effect of catalytic activation of nickel is more prominent, and thus led to better hydrogen storage. Hence, it was concluded that hydrogen storage capacity was related to micropore volumes, Pore size distribution (PSD) and surface properties of ACFs as well as specific surface areas.

Keywords: Adsorption; Porosity; Surface treatment; Fluorination; Nickel doping; Activated carbon fiber; Hydrogen storage

1. Introduction

Hydrogen storage on carbon materials has recently been attracting attention because of the importance of hydrogen as an energy carrier in automotive applications. In order to improve the hydrogen storage capacity of carbon materials, various methods have been suggested [1–4]. Some theoretical research by Monte Carlo simulation and other calculations have supported this finding [4,5]. Especially novel carbon materials, such as carbon nanotubes, activated carbon and carbon nanofibers have attracted a lot of interest. However, the values for their hydrogen storage capacity scatter over several orders of magnitude [6]. The reasons for the discrepancy among recent reports with respect to hydrogen storage capacity of carbon materials can be considered to be the difference among evaluation techniques, and experimental errors owing to the difficulty of evaluation. In addition, the mechanism of hydrogen storage and the interaction between the carbon surface and hydrogen are not adequately understood. Therefore, the hydrogen storage properties of carbon materials must be analyzed accurately by using well-characterized samples to evaluate the capacity of hydrogen storage in carbon materials as well as an appropriately designed structure to enhance the storage capacity [7]. Recently, metal doping has drawn much attention as some selected metals enhance hydrogen storage due to the formation of active sites on the carbon materials, enhancing hydrogen adsorption [8–11]. Fluorine additions to MgH_2 nanocomposites are also beneficial with respect to the H-sorption behavior due to the catalytic activity of fluorine. The formation of a fluorinated surface layer enhances hydrogen reactivity and protects the material from passivation [12]. Activated carbon fibers (ACFs) exhibit a greater adsorption rate and adsorption capacity than the usual granulated activated carbons (AC) and so can adsorb a mass of chemical substances in gas and liquid phases.

In this study, activated carbon fibers have been surface modified by transition metal Ni doping or fluorination,

* Corresponding author. Tel.: +82 42 821 7007; fax: +82 42 822 6637.
E-mail address: youngslee@cnu.ac.kr (Y.S. Lee).

0920-5861/$ – see front matter © 2006 Elsevier B.V. All rights reserved.
doi:10.1016/j.cattod.2006.09.014

characterized and investigated to assess of their adsorption capacity and pore characteristics. The high-pressure adsorption apparatus was made with sufficient accuracy. In order to understand the nature of the pore and the adsorption process of surface modified ACFs, the hydrogen storage capacity is correlated with the structural properties of the ACF samples. From these results, we determined the relationship between the storage capacity and the pore structures of the activated carbon fiber samples. Preliminary results for activated carbon fibers modified by Ni or F_2, chosen in order to investigate the catalytic effect of transition metals and the possible benefits of fluorination, are reported.

2. Experimental

2.1. Activated carbon fibers

The starting material samples used in this study were the activated carbon fibers (ACFs) designated ACF-15 (namely, R-A15). ACFs were supplied by Osaka Gas Chemical Co. Ltd. The activated carbon fibers used were washed several times with distilled water and dried in a vacuum oven at 85 °C for 24 h.

2.2. Fluorination of ACF samples

The reaction between activated carbon fibers (ACFs) and fluorine is highly exothermic [13]. The unrestricted reaction can proceed briskly, thus causing a rapid heating that can easily inflame the activated carbon fiber to form carbon–fluorine compounds. The surface fluorination of ACFs was performed following a process known to be efficient for the fluorination of activated carbon fibers [14–16]. To control the rate of fluorination and allow the heat of reaction to dissipate, F_2–N_2 gas mixture was used at room temperature. Fiber bundles, weighing 400 mg, were loaded into a fluorine-passivated nickel reactor (2 in. i.d.) sealed by a PTFE gasket.

The activated carbon fiber was preconditioned by heating to 200 °C under flowing nitrogen. Fluorine gas was supplied by Messer Griesheim (purity 99.8%). The balance was almost all nitrogen with the amount of hydrogen fluoride impurity under 0.01%. The trace amount of hydrogen fluoride was removed by sodium fluoride pellets heated at 100 °C. The system was evacuated for about 2 h, and then diluted fluorine was introduced into the reactor at a very low flow. Activated carbon fibers were allowed to react with fluorine for 30 min at mole fractions of 0.1 (namely F1-A15), and 0.2 (namely F2-A15). After the reaction, the reaction vessel was then pumped out again to 10 mTorr with subsequent nitrogen gas purge prior to the extraction of the fiber bundles.

2.3. Nickel doping of ACF samples

The activated carbon fiber samples were impregnated with nickel nitrate ($NiNO_3$) acetone solutions by a vacuum decomposition process using the incipient wetness impregnation method [17]. In this study, a nickel nitrate solution (analytical grade) of a low concentration (5 mM) was selected for the vacuum impregnation process. ACFs impregnated with the acetone solution were then filtered and dried at 60 °C for 4 h. The resultants ACF (namely Ni-A15) doped with Ni were then heated at 100 °C for 1 h under hydrogen atmosphere to reduce the nickel salt to nanoparticles.

2.4. Characterization of fluorinated and Ni-doped ACFs

The samples were characterized using low temperature (77 K) nitrogen adsorption isotherms measured over a wide range of relative pressures from 10^{-6} to 1. Adsorption measurements were performed on a Micromeritics ASAP 2020 automatic adsorption apparatus. High purity nitrogen (99.99%) was used. Prior to measurement, the samples were degassed at 423 K for 10 h in the degas port of the adsorption analyzer. The specific surface area, pore volume, and pore size distribution (PSD) were determined by the BET and *t*-plot methods. The formation of pores in ACF is closely associated with the defects of the graphite-like crystal layers in ACF. The XRD patterns (D/MAX-2400, Rigaku Co., Japan) of the graphite-like crystal structure of the samples were studied. The changes in pore size were influenced by the crystal interlayer distance. The radiation used was Cu Kα X-rays operated at 36 kV and 80 mA.

2.5. Hydrogen storage measurement

Hydrogen adsorption capacities at 303 K over the hydrogen pressure range up to 100 bar were measured by the PCT method (AnySorb 7) with an automatically controlled apparatus for high-pressure adsorption. The hydrogen adsorption capacities were measured after all samples were pretreated at 423 K for 90 min in helium flow and sequentially reduced in situ in a hydrogen/nitrogen mixture flow. High-purity hydrogen (99.999%) was used in this study. The amounts of hydrogen adsorbed were calculated using the Redlich/Kwong equation.

Steps were taken to ensure the accuracy of the experimental results. The principal part of the apparatus was held in an air thermostat to keep its temperature at 303 K. The apparatus was previously tested for leakage and calibrated with the empty sample cell and well-known standard samples (MSC-30). The time adopted for equilibration was 30 min at each step. About 300 mg of the activated carbon samples were used for hydrogen adsorption.

3. Results and discussion

3.1. Microstructural properties of modified ACFs

Fig. 1 shows the nitrogen adsorption isotherms for the untreated and surface modified ACFs. Detailed information on the textural properties of the samples is listed in Table 1. By IUPAC classification, pores are classified as micropores, mesopores and macropores [18]. The volumes of micropores were obtained by the *t*-plot [19] and α_s-plot [20]. Surface

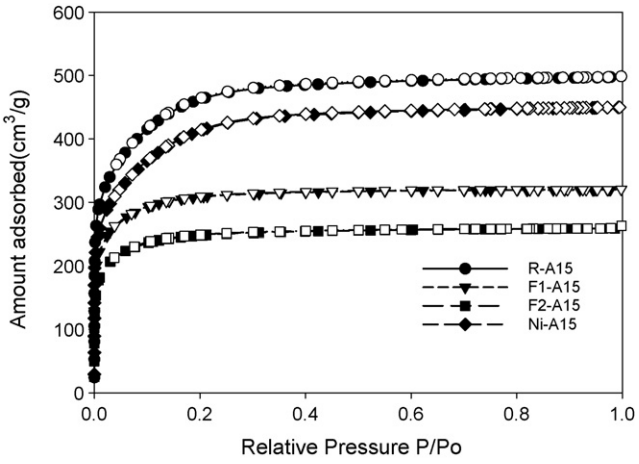

Fig. 1. N_2 adsorption isotherms (77 K) of the ACFs used in this study.

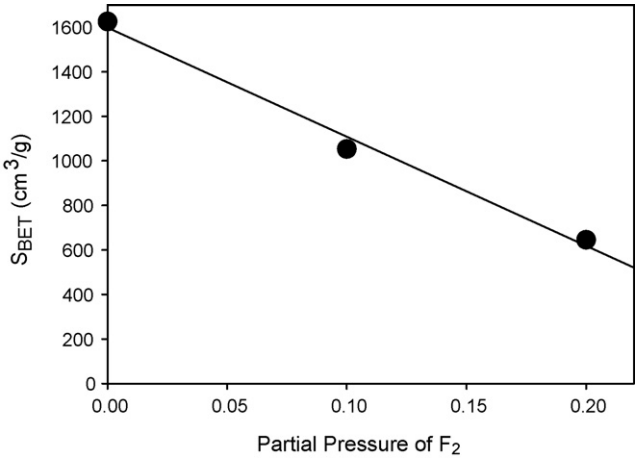

Fig. 2. BET specific surface area of fluorinated ACFs according to the partial pressure of F_2.

areas of mesopores (including the contributions from the external pore area) were also determined by the *t*- and α_s-plot. There are six kinds of adsorption isotherms by the IUPAC classification, and each indicates a distinct pore structure. Therefore, the shape of the adsorption isotherm is very important in adsorption using ACFs as the adsorbent. The adsorption isotherms of all samples, as seen in Fig. 1, are still classified as type I, similar to the starting sample R-A15. This signifies that the samples are microporous ones. It is also shown in Fig. 1 that as ACFs were modified, the amount of N_2 adsorbed gradually decreased from Ni-A15 to F1-A15 to F2-A15. It is evident that most of the pore volume of samples is filled below a relative pressure of about 0.1, indicating that these ACFs are highly microporous. After a sharp increase up to relative pressure 0.1, a small amount of N_2 began to be adsorbed within the large pores or on the external surface. Table 1 summarizes these results.

Fig. 2 shows the relationship between the specific surface area (S_{BET}) and partial pressure of fluorinated ACFs. As shown in Fig. 2 and Table 1, the specific surface area and total pore volume of fluorinated ACFs significantly decrease with increasing degree of fluorination. These results agree with those reported by other researchers [21,22]. However, the meso/micropore volume ratio is also somewhat decreased with fluorination. This result indicates that the fraction of micropores may be increased with fluorination. It may now assumed that the fluorination plays the role not only destroys mesopores but also blocks (or narrows) mesopores by fluorine-functional groups which formed by fluorination.

The formation of pores in ACFs is due to the existing defects of the graphite-like crystal layer; therefore, the pore shape should be slit-like, not cylindrical or other geometries [23,24]. Hence, the slit-like pore model is more appropriate for the pores in ACFs. The average pore width, W_{AVP}, can be also obtained from the E_0 value by the so-called Dubinin–Stoeckli (DS) relation (results shown in Table 1). Several forms of the DS relation are known [25,26]. The newest one is described by Eq. (1) [27]:

$$W_{AVP} = \frac{10.8}{E_0 - 11.4} \quad (1)$$

where E_0 is the characteristic adsorption energy expressed in the DR equation. Eq. (1) is based on the DR equation with the adsorption mechanism of micropore volume filling. As shown in Table 1, fluorination narrows the pores of ACFs; this effect is more prominent than that of Ni-doping used in this study.

Table 1
Pore structure parameter of the ACFs used in this study

Sample	S_{BET}[a] (m^2/g)	V_t[b] (cm^3/g)	V_{mi}[c] (cm^3/g)		V_{me}/V_{mi}[d]	S_{EA}[e] (m^2/g)		W_{AVP}[f] (nm)
			t-Plot	α_s-Plot		*t*-Plot	α_s-Plot	
R-A15	1626.0	0.770	0.745	0.739	0.034	20.3	17.0	2.86
F1-A15	1053.4	0.495	0.482	0.485	0.027	13.7	5.6	2.35
F2-A15	645.7	0.400	0.391	0.378	0.023	7.8	15.0	2.22
Ni-A15	1467.7	0.696	0.661	0.664	0.053	33.6	17.9	2.63

[a] BET surface area.
[b] Total pore volume.
[c] Micropore volume.
[d] Meso/micropore volume ratio.
[e] External surface area.
[f] Average pore width.

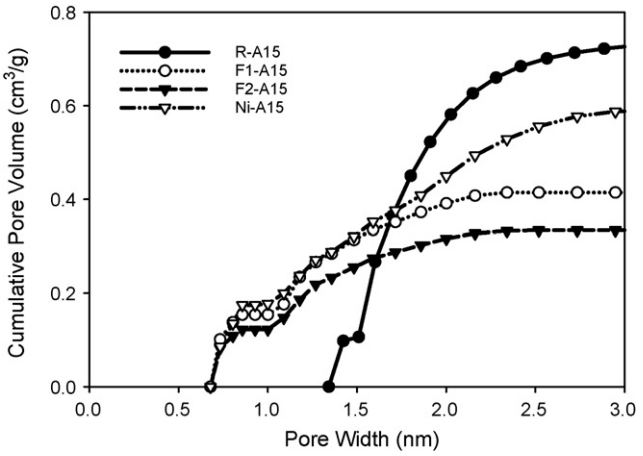

Fig. 3. Relationship between cumulative pore volume and pore width of ACFs used in this study.

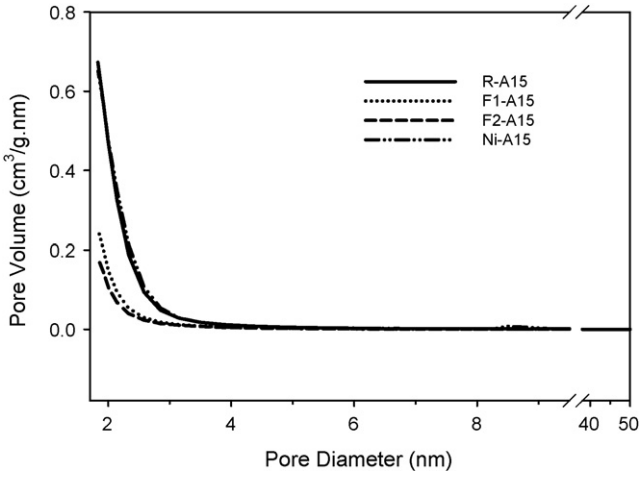

Fig. 5. The mesopore PSD of the ACFs by the BJH method.

3.2. Analysis of PSD of ACFs

As one of the pore characteristic parameters, PSD influences the equilibrium of adsorption and transport of fluids. Other pore parameters such as surface area and pore volume can be also obtained from information on PSD. Fig. 3 shows the pore size distributions for the surface modified ACFs as well as for the R-A15 ACFs. All samples possess primarily micropores, which, according to the IUPAC classification, have widths below 2 nm [18]. For all samples, cumulative pore volume suggested predominance of micropores. It is also found that the total micropore volume of the surface modified ACFs decreased, as already shown in Fig. 3 and Table 1. However, average pore width (W_{AVP}) is not significantly changed by surface modification, although micropore volume is decreased. In order to comprehensively understand the effects of surface modification, especially fluorination, on the pore wall, it is necessary to determine in detail the PSD of mesopores, as well as the PSD of micropores. As shown in Fig. 1, all samples are microporous materials, so their PSDs can be analyzed by the MP method.

Fig. 4 shows the micropore PSDs (by MP method) of samples. When the ACFs were fluorinated, the range of the pore size distribution gradually narrowed from R-A15 to fluorinated ACFs. On the other hand, that of Ni-A15 is nearly unchanged. It is believed that the fluorination of ACFs can possibly narrow the pore size to some extent. Its controlling effect on pore size is not prominent on account of a large number of mesopores and macropores being formed simultaneously on the surface [23]. The PSDs of mesopores obtained by the BJH method in all samples are shown in Fig. 5. As shown in Fig. 5, the volume and surface area of mesopores gradually decreased from R-A15 and Ni-A15 to F1-A15 and F2-A15; the mesopore size distribution is mainly in the range of 2–5 nm, whereas pores with a size larger than 50 nm did not even exist.

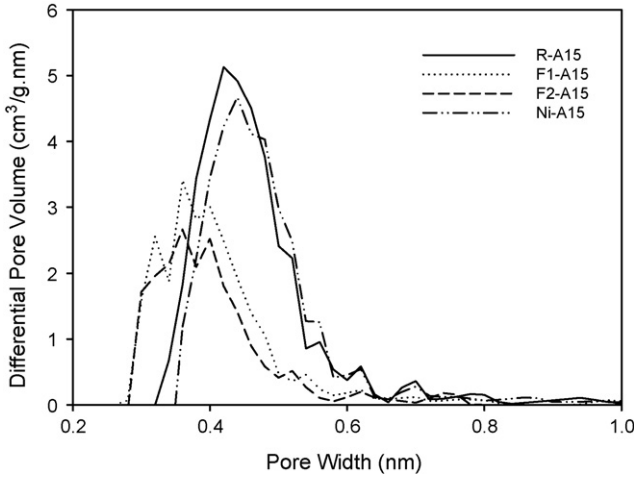

Fig. 4. The micropore PSD of the ACFs by the MP method.

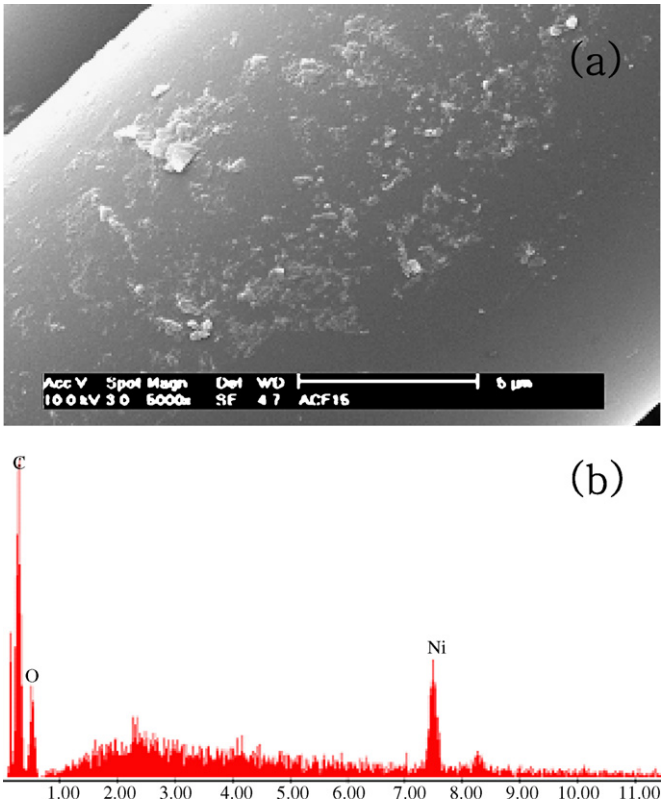

Fig. 6. SEM image (a) and EDS data (b) of Ni doped ACFs.

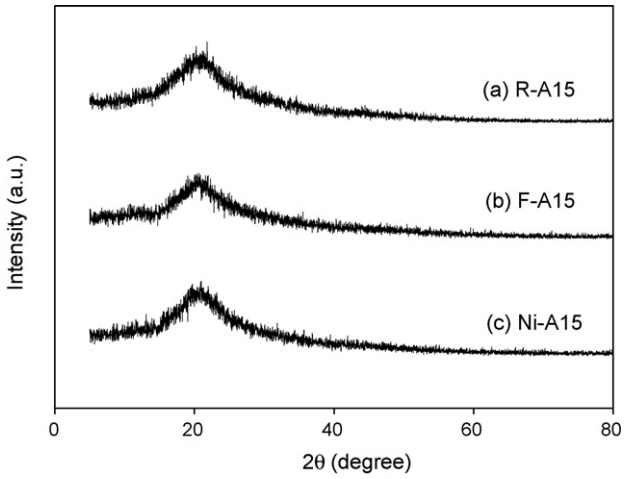

Fig. 7. XRD patterns of the ACFs.

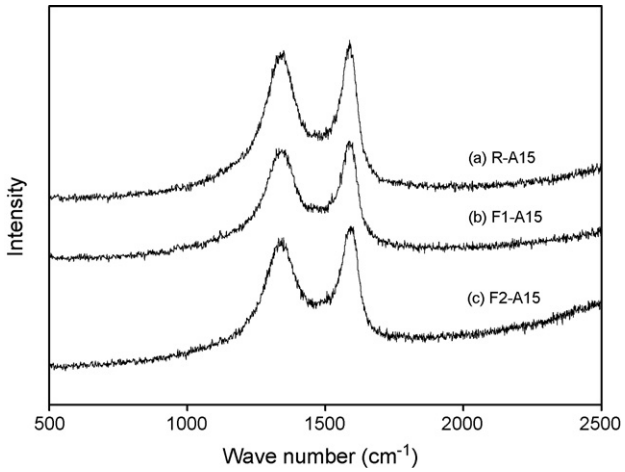

Fig. 8. Raman spectra of the ACFs.

3.3. Surface morphology and nanostructural changes of modified ACFs

From Fig. 6, which shows the scanning electro microscope (SEM) images and energy dispersion spectroscopy (EDS) of the Ni-doped ACFs, we see the Ni powder dispersed onto the surface of ACFs. From an EDS, only three elements, C, O and Ni, could be found. No other impurities were detected in the nanostructures. From the SEM results, it seems that some of the coating metals had covered the surfaces of the fibers. The average bulk structure of carbon materials can be readily revealed using X-ray diffraction. The wide-angle XRD patterns of the ACFs studied are shown in Fig. 7. As listed in Table 2, broad diffraction peaks at low diffraction angles corresponding to 2θ at 20–22° are observed; these are assigned to the disordered graphitic (0 0 2) plane. The location and breadth of this peak indicate that activated carbon fibers have a coke-like character with a disordered carbonaceous interlayer [28]. Meanwhile, it is well known that XRD is a powerful technique for examining the detailed microstructure of carbonaceous materials, such as the interlayer spacing ($d_{0\,0\,2}$) of the ACFs. This is composed of small layers with the same atomic positions as graphite within the layers [29,30].

In this work, the interlayer spacing of modified ACFs is between 4.239 and 4.317 Å and that of the untreated ACFs (R-A15) is 4.070 Å, as shown in Table 2. The carbon basal planes are changed by Ni-doping and fluorination treatment. The interlayer spacing of all of the samples is higher than that of graphite (3.354 Å) because activated carbon fibers are less-ordered material [31]. No signature of nickel in the Ni-doped ACFs sample has been observed due to the small amount in the XRD analysis (Fig. 7). However, the nickel signature of Ni-doped ACFs has already been observed in SEM/EDS results (Fig. 6). The XRD peak intensity of the carbon structure (2θ value of 21.82°) decreased with the surface of ACFs.

Table 2
Results of XRD measurements of the ACFs

Sample	2θ (°)	$d_{0\,0\,2}$ (Å)
R-A15	21.82	4.070
F-A15	20.94	4.239
Ni-A15	20.56	4.317

Fig. 8 shows the Raman spectra of the ACFs used in this study. The spectra, characterized by two peaks at 1350 and 1580 cm^{-1}, are typical to the high wave-number region of ACFs. These peaks are associated with disorder-induced (D-band) and tangential graphitized carbon (G-band), respectively. The integrated intensity ratio (R) between D- and G-band, i.e., I_D/I_G of ACFs (R-A15) is found to be 0.945. In Fig. 8, the relative intensity ratio R ($I_{1350\,cm^{-1}}/I_{1580\,cm^{-1}}$) of each ACF is calculated. The R-value estimated by Raman spectroscopy also indicates the relative quantity of structural defects in ACFs. In Fig. 8, the R-values of fluorinated ACFs were 0.965 and 0.936 for F1-A15 and F2-A15, respectively, and almost the same as that of R-A15. This indicates that no defects by fluorination were introduced into the starting ACFs.

3.4. Hydrogen storage capacity

We estimated the hydrogen storage capacity of modified ACFs with the PCT method. Fig. 9 shows hydrogen adsorption isotherms of ACFs studied over hydrogen pressure up to

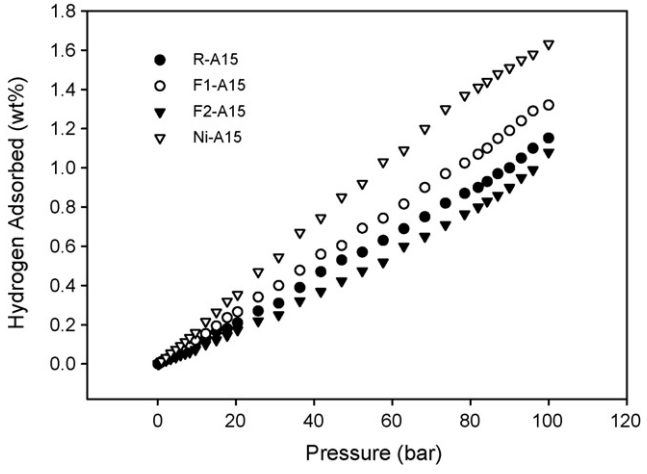

Fig. 9. Representative hydrogen adsorption isotherm of the ACFs at 303 K.

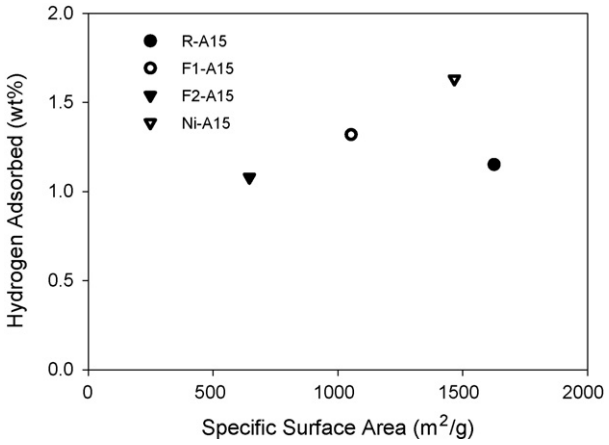

Fig. 10. Effect of specific surface area on the hydrogen adsorption capacity of the ACFs at 100 bar, 303 K.

100 bar. We have obtained similarly shaped of hydrogen adsorption isotherms in spite of surface modification for all ACFs studied. Hydrogen adsorption capacity is a linear function of pressure, which can be explained by Henry's law. These results indicated that nickel was well dispersed on the surface of activated carbon fibers. The amount of hydrogen adsorbed increased with increasing pressure. The amounts of hydrogen adsorbed on nickel doped activated carbon fibers were much larger than those for activated carbon fibers. In the data shown in Table 1 and Fig. 9, the effect of catalytic activation of nickel is more prominent, and thus led to more hydrogen storage. It could be confirmed that surface modification of ACFs plays an important role in determining the porous structure and amounts of hydrogen adsorbed. Fig. 10 shows the effect of specific surface area on the hydrogen adsorption capacity of the all ACFs studied at 100 bar, 298 K. As the BET surface area increases, the hydrogen adsorption of the materials also increases [32]. In this study, though the specific surface areas of modified ACFs are decreased, their hydrogen adsorption are improved as compared with unmodified ACFs due to the enhancement of hydrogen affinity by Ni doping and fluorination.

4. Conclusions

Activated carbon fibers (ACFs) with high surface area and pore volume have been modified by metal (Ni) doping and fluorination for improved hydrogen storage. When ACFs were fluorinated, the range of the pore size distribution gradually narrowed. The XRD peak intensity of the carbon structure (2θ value of 21.82°) decreased upon modification of the surface of ACFs. After fluorination treatment, although the micropore volume of ACF was decreased, hydrogen uptakes were found to be higher than those measured at the same conditions without fluorination. We also found that the micropore volume of ACFs was not substantially changed with Ni doping. Hydrogen storage capacities were considerably higher due to the effect of catalytic activation of nickel. Though fluorination of ACFs produces higher hydrogen affinity, the effect of catalytic activation of nickel is more prominent, and thus led to more storage of hydrogen.

Acknowledgements

This research was performed for the Hydrogen Energy R&D Center, one of the 21st Century Frontier R&D Program, funded by the Ministry of Science and Technology of Korea.

References

[1] A.C. Dillon, K.E.H. Gilbert, J.L. Alleman, T. Gennett, K.M. Jones, P.A. Parilla, M.J. Heben, in: Proceedings of the 2001 DOE Hydrogen Program Review, NREL/CP-570-30535, 2001.
[2] E. David, J. Mater. Proc. Technol. 162/163 (2005) 169.
[3] G.G. Tibbetts, G.P. Meisner, C.H. Olk, Carbon 39 (2001) 292.
[4] H.M. Cheng, Q.H. Yang, C. Liu, Carbon 39 (2001) 1447.
[5] Q. Wang, J.K. Johnson, J. Chem. Phys. 110 (1999) 577.
[6] B. Panella, M. Hircher, S. Roth, Carbon 43 (2005) 2209.
[7] H. Takagi, H. Hatora, Y. Yamada, Carbon 43 (2005) 3037.
[8] P. Chen, X. Wu, J. Lin, K.L. Tan, Science 285 (1999) 91.
[9] Z.H. Zhu, G.Q. Lu, S.C. Smith, Carbon 42 (2004) 2509.
[10] S. Challet, P. Azais, R.J.-M. Pellenq, O. Isnard, J.-L. Soubeyroux, L. Duclaux, J. Phys. Chem. Solids 65 (2004) 541.
[11] K. Kim, H. Lee, K. Han, J. Kim, M. Song, M. Park, J. Lee, J. Kang, J. Phys. Chem. B 109 (2005) 8983.
[12] S. Deleddaa, A. Borissovaa, C. Poinsignona, W.J. Bottaa, M. Dornheimb, T. Klassenb, J. Alloys Compd. 404–406 (2005) 409.
[13] T. Nakajima, N. Watanabe, Graphite Fluorides and Carbon–Fluorine Compounds, CRC Press, Boca Raton, FL, 1990 (Chapter 3).
[14] Y.S. Lee, T.H. Cho, B.K. Lee, J.S. Rho, K.H. An, H.Y. Lee, J. Fluorine Chem. 120 (2003) 99.
[15] I.S. Lim, S.H. Yoo, I.N. Park, Y.S. Lee, Carbon Sci. 5 (2004) 12.
[16] Y.S. Lee, B.K. Lee, Carbon 40 (2002) 2461.
[17] H. Bönnemann, K.S. Nagabhushana, in: H.S. Nalwa (Ed.), Encyclopedia of Nanoscience and Nanotechnology, American Scientific Publishers, 2004, p. 777.
[18] K.S.W. Sing, D.H. Everett, R.A.W. Haul, L. Moscou, R.A. Pierotti, Pure Appl. Chem. 57 (1985) 603.
[19] J.H. de Boer, B.C. Lippens, B.G. Linsen, J.C.P. Broekhoff, A. van den Heuvel, J. Colloid Interface Sci. 21 (1966) 405.
[20] S.J. Gregg, K.S.W. Sing, Adsorption Surface Area and Porosity, 2nd ed., Academic Press, New York, 1982, pp. 94–102.
[21] G.D. Del Cul, L.D. Trowbridge, L.M. Toth, J.N. Fiedor, J. Fluorine Chem. 101 (2000) 137.
[22] D.T. Cronce, A.A. Mansour, R.P. Brown, B.C. Beard, Carbon 35 (1997) 483.
[23] J. Xin, X. Wang, J. Deng, Micropor. Mesopor. Mater. 76 (2004) 167.
[24] A. Bailey, D.H. Everett, Nature 211 (1966) 1082.
[25] J. Sun, Carbon 40 (2002) 1051.
[26] C.L. Mangun, K.R. Benak, J. Economy, K.L. Foster, Carbon 39 (2001) 1809.
[27] F. Stoeckli, A. Slasli, D. Hugi-Cleary, A. Guillot, Micropor. Mesopor. Mater. 51 (2002) 197.
[28] K. Kinoshita, Carbon, Electrochemical and Physicochemical Properties, Wiley, New York, 1988.
[29] I. Medalla, Carbon Black—Polymer Composites, Marcel Dekker, New York, 1984.
[30] N.S. Ahmadi, F.A. Khonsari, J. Amouroux, J. Mater. Chem. 5 (1995) 229.
[31] S.J. Park, Y.S. Jang, J. Colloid Interface Sci. 261 (2003) 238.
[32] J.M. Blackman, J.W. Patrick, C.E. Snape, Carbon 44 (2006) 918.